Journal of Electroceramics 3:1, 73–83, 1999


# Microassembly of a Piezoelectric Miniature Motor

MATS BEXELL & STEFAN JOHANSSON
*Department of Materials Science, Uppsala University, Box 534, S-751 21 Uppsala, Sweden*

Submitted December 5, 1997; Revised August 25, 1998; Accepted September 3, 1998

**Abstract.** An assembly method for the fabrication of a piezoelectric miniature motor is presented. The fabrication is done by placement and soldering of piezoceramic elements onto a silicon substrate. The assembly of the miniature motor demands high precision ($\pm 5\,\mu$m), four-axes positioning which is fulfilled by a special micropositioning stage. A particular assembling sequence is used and critical process and performance parameters are evaluated. One of the important factors is the joint strength between the piezoceramic element and the silicon substrate. A joint strength as high as 100 MPa has been measured which would allow for torque values in the range of 14 mNm for a 4 mm diameter motor.

**Keywords:** microassembly, miniature motor, piezomotor, piezoelectric, micropositioning

## 1. Introduction

There is an increasing interest in miniaturized actuators for applications in areas such as medicine and automation. It will take some time, however, before any micro-technology based actuator is found on the commercial market. Among the technical reasons for this is the need for further development of the process technology. This article addresses this issue and in particular an assembly technique for piezoceramic elements that can be used in miniature motors.

To comply with most of the desired characteristics in a miniature actuator system (e.g., high output forces, large stroke length and easy fabrication) a new piezoelectric motor design has been developed [1]. The driving principle of the motor is a rotating ''inchworm'' mechanism [2]. In contrast to ultrasonic motors based on resonance [3], the motor is based on quasistatic positioning of piezoceramic elements. In our motor design, Fig. 1, piezoceramic elements with two axial motion capacity are used to simplify the motor construction. The two modes of motion used are bending and extension/contraction of the piezoceramic elements. By combination of these two modes a rotor can be moved in a stepwise (''inchworm'') manner using the friction forces between the piezoceramic elements and the rotor. The piezoceramic elements are PZT multimorphs, i.e., multilayer piezoceramic elements connected electrically to behave as bimorphs. A simple bimorph consists of two piezoelectric layers, see Fig. 1, with one intermediate and two external electrodes. In a bimorph it is possible to activate the electric field in each layer independent of the other. Using phase shifted sinusoidal fields in the two layers the bimorph's end move along an elliptical trajectory. A planar motor can be constructed by using two sets of piezoceramic elements that operate with a phase difference of 180°. Three piezoceramic elements in each of the two sets (indicated at the right hand side of Fig. 1) ensure stability of the planar rotor since there are always three piezoceramic elements in contact with the rotor during a drive cycle. The performance of a first prototype miniature motor with diameter 4 mm has been evaluated [4]. Experiments showed that the motor principle worked well on a miniature scale and a high output torque (maximum of 1.4 mNm) was confirmed. A miniature motor of the same size as the one evaluated but with a more optimized design could possibly reach torque and rotational speed values above 10 mNm and 200 rpm.

To combine different materials in miniature actuator systems, some type of assembly technique

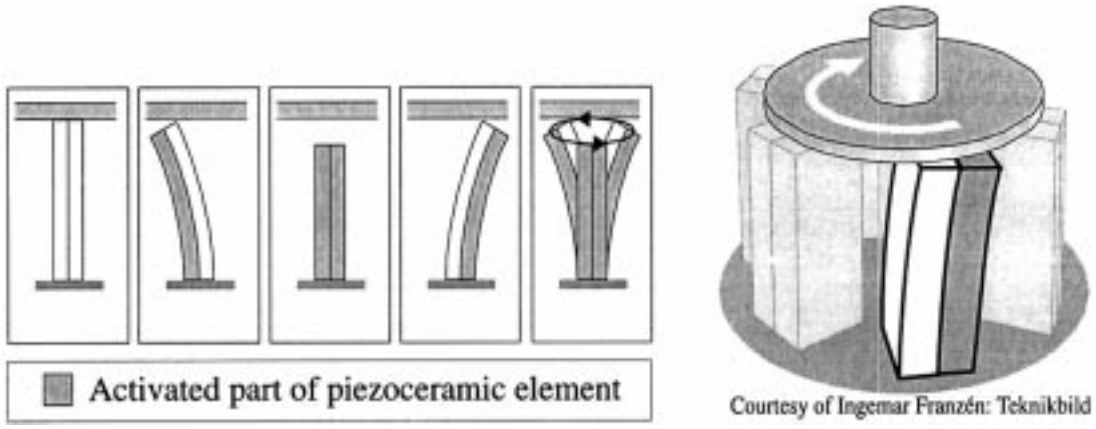


*Fig. 1.* Motion capacity (left hand side) of a piezoceramic bimorph element and (right hand side) a planar rotating motor construction where bimorph elements operate three at a time.

is usually required [5]. In particular when piezoceramic elements are assembled, the critical factors for system performance will be both the electrical and the mechanical properties of the joint. The process technique chosen for fabrication of the miniature motor is microassembly by soldering piezoceramic elements on a silicon substrate. The choice of silicon as substrate material makes it possible for future integration of drive electronics for the piezoceramic elements. This technique is believed to be a realistic way to fabricate miniature motors commercially. The process can be performed in air without extreme demands on environmental conditions (e.g., clean room facilities) which in a commercial process is of great advantage. In this particular case the electrical conditions in the joint is fulfilled by the soldering procedure. For further enhancement of the mechanical properties of the joint an adhesive is incorporated in the space between the silicon substrate and the piezoceramic element. These underfills are commonly used in flip-chip assembly for improvement of joint properties of the soldered components [6].

This article presents the assembly equipment and data for process parameters in the microassembly procedure. The main objectives for the experiments carried out were an evaluation of the demands on resolution and precision in assembly and identification of critical fabrication steps. Among those is the joint strength between the silicon substrate and the piezoceramic element. The joint strength could, for instance, limit the maximum torque level of the motor.

## 2. Motor Components

One of the few realistic fabrication techniques for complex micro- or miniature systems today is using high precision assembly. From an economic point of view, it is advantageous to reduce the number of components in the system to a minimum. The motor consists of five major parts, a base plate, a stator, a rotor, a ball bearing and a housing, Fig. 2. The base plate is used to keep the stator fixed relative to the rotor and to adjust the contact force between stator and rotor by screwing the base plate into the housing. Glued onto the rotor is a wear-resistant material, a sapphire plate, with an extremely flat surface. Base plate, housing and rotor are all made by high precision turning in stainless steel.

The stator of the miniature motor consists of a silicon substrate with an electrode pattern and six piezoceramic elements. Each piezoceramic element have dimensions $1.5 \times 1.05 \times 0.9\,\text{mm}$ ($h \times w \times t$, see Fig. 12) and consists of alternating layers of active material (PZT) and silver/palladium electrodes. The electrode distance is about $56\,\mu\text{m}$ (14 active layers) and the electrode thickness is 3 to $4\,\mu\text{m}$. The piezoceramic elements have been made by cutting (dice sawing) a large multilayer PZT plate (which is poled) into smaller piezoceramic elements, which thereafter have been polished to equal dimensions (accuracy of $\pm\,5\,\mu\text{m}$).

The two layer electrode pattern on the silicon (Si) substrate is made by standard lithographic techniques. A first electrode layer of 2000 Å aluminum is

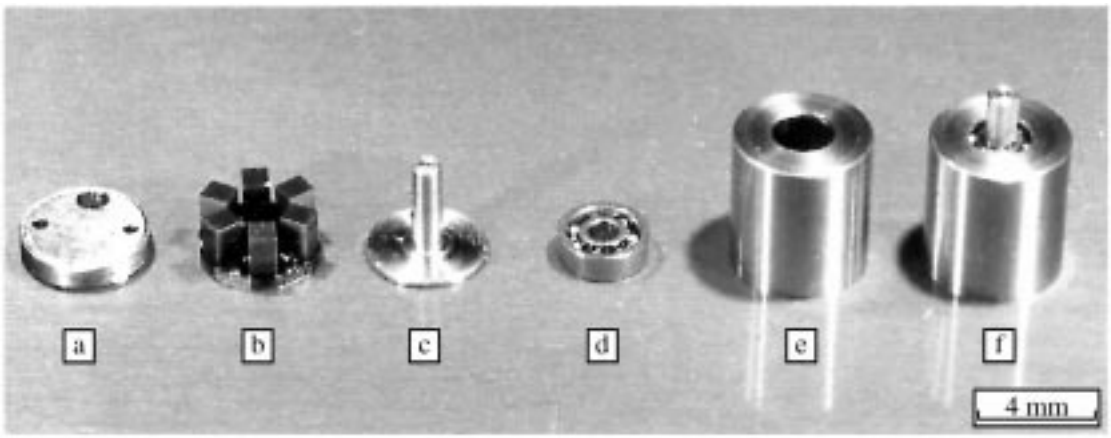


*Fig. 2.* Motor details, (a) base plate, (b) stator, (c) rotor, (d) ball bearing, (e) housing and (f) a fully assembled motor.

deposited by electron beam evaporation onto a bottom layer of thermal oxide. As insulation between the electrode layers, an 8000 Å low temperature $SiO_2$ (LTO) layer is used. The via-holes in the LTO for electrical connection between the electrode layers have been made by reactive ion etching. The second electrode layer consists of 500 Å Ti/2000 Å Ni electron beam evaporated thin films. Titanium is used as an adhesion layer on the LTO and nickel is used as a seed layer for an approximately 5 $\mu$m thick electroplated tin/lead solder of eutectic composition. The electrodes in every electrode area are connected in such a way that the piezoceramic elements will behave like piezoelectric bimorphs when an electric voltage is applied to them, see Fig. 3. The design of the electrode pattern is shown in Fig. 4(a). Figure 4(b) shows one of six electrode areas where electrodes in one piezoceramic element are soldered against the corresponding electrodes in the electrode pattern.

## 3. Assembly Equipment

The equipment used for assembly of the miniature motor is shown in Fig. 5. It consists of (a) a vacuum tool with a force cell for handling of the piezoceramic elements, (b) a heating table with (c) an alignment corner and (d) a micropositioning stage. These components are described in more detail in the following.

The micropositioning stage allows high precision, four-axes positioning with a centimeter workspace. The *xyz*-axis positioning resolution is 10 nm, the rotational resolution 8.7 $\mu$rad and the travelling range

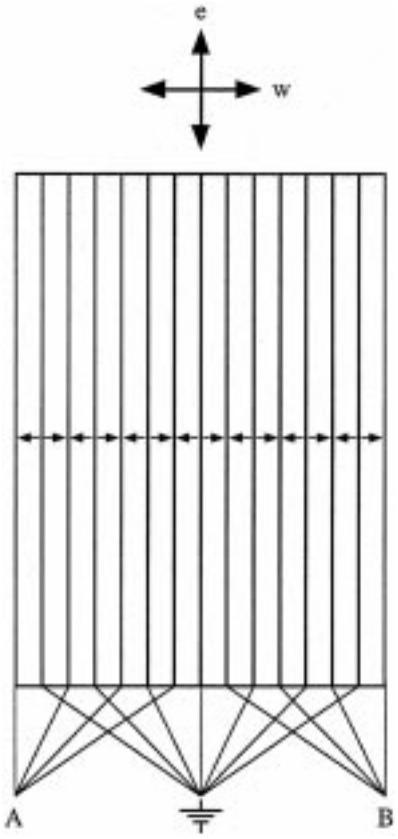


*Fig. 3.* Schematic drawing of the piezoceramic element showing how the layers are connected to drive voltages A, B and earth in order to behave like a piezoelectric bimorph. Depending on how the applied voltages are combined, the tip of the piezoceramic element can either bend or extend/contract, denoted with w and e respectively. Arrows indicate the direction of polarization in each layer of the piezoceramic element.

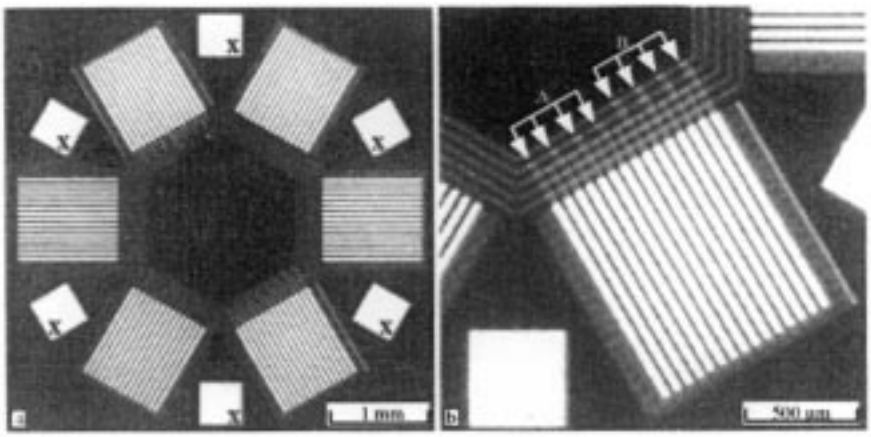

*Fig. 4.* (a) The electrode pattern design and (b) one of the electrode areas where piezoceramic elements are soldered. The hexagonal pattern in (a) is the bottom aluminium electrode layer. The arrows in (b) show where connections are made (via-holes) to the upper electrode layer. Electrodes denoted with (A) are connected with one phase and (B) with the other phase in a piezoceramic element. Earth electrodes are those not marked in the figure (every second). Marked with a cross (X) are the bonding pads where electrical leads (insulated copper wires) are connected to the electrode pattern.

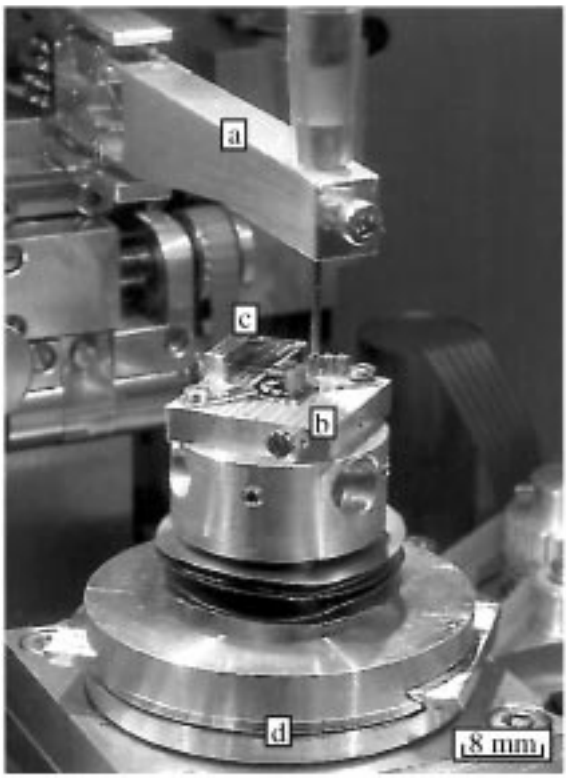


*Fig. 5.* The assembly equipment. Seen are the vacuum tool with its force cell (a), the heating table (b) with its alignment corner (c) and the connector to the positioning stage (d). The photograph is taken when three piezoceramic elements have been assembled.

10–25 mm for all the linear axis. All axes are equipped with a piezoelectric actuator which is used for fine adjustment of position. In the experiments, positioning of the table is controlled manually with a joystick and supervision of movements is made with an optical stereo microscope. Absolute values of position for all four axes are measured with optical encoders. The micropositioning table can be oscillated in linear directions by use of the piezoelectric actuator with a maximum amplitude and frequency of $\pm 7\,\mu$m and 100 Hz. During assembly, the micropositioning table has been oscillated sinusoidally in one linear ($y$-) direction.

A specially designed heating unit is connected to the micropositioning stage. It is made of aluminum and is heated resistively. The heating unit is placed on a tripod made of aluminum oxide tubes. Heat shields made of titanium foil are placed between the heating unit and the base plate to protect the components in the micropositioning stage from heat radiation. The temperature is measured with a thermocouple put into the heating unit, close to its upper surface. The silicon substrate, where piezoceramic elements are soldered, is mechanically clamped onto the heating unit with metal clips. An alignment corner on the heating unit is used to align piezoceramic elements during assembly. A well defined surface on the two vertical sides is achieved by gluing silicon plates with a two component epoxy resin (EPO-TEK 377) which can

withstand long term use at elevated temperatures (at the soldering temperature) without degrading [7].

A vacuum tool, equipped with a force cell for measurement of contact force between silicon substrate and piezoceramic elements during soldering is used to handle the piezoceramic elements. The force cell with a resolution of 1 mN has a double cantilever design to reduce tool rotation. The tip of the vacuum tool is polished flat and the inside opening area of the vacuum tube is chosen to be as large as possible in order to achieve as high holding force as possible onto the piezoceramic elements. The deviation angle between the *xy*-plane of the positioning table and the vacuum tool tip is measured in the stereo microscope with aid of a plane parallel plate held by the vacuum tool. The deviation error is minimized by mechanical adjustment.

## 4. Microassembling Sequence

A particular assembling sequence has been used for fabrication of the stator in the piezoelectric miniature motor. The assembling sequence is summarized in the flow chart given in Fig. 6, and the photographs illustrate some of the fabrication steps. The procedure begins with increasing the temperature to the soldering temperature (215 °C) to minimize effects from thermal expansion of the heating unit and the silicon substrate. An active liquid flux (Multicore PC 29–17) is applied on the silicon substrate surface before heating in order to react with the oxide layer on the solder alloy, protect the tin/lead solder from further oxidation and promote solder wetting on the Ag/Pd electrodes in the piezoceramic element during assembling.

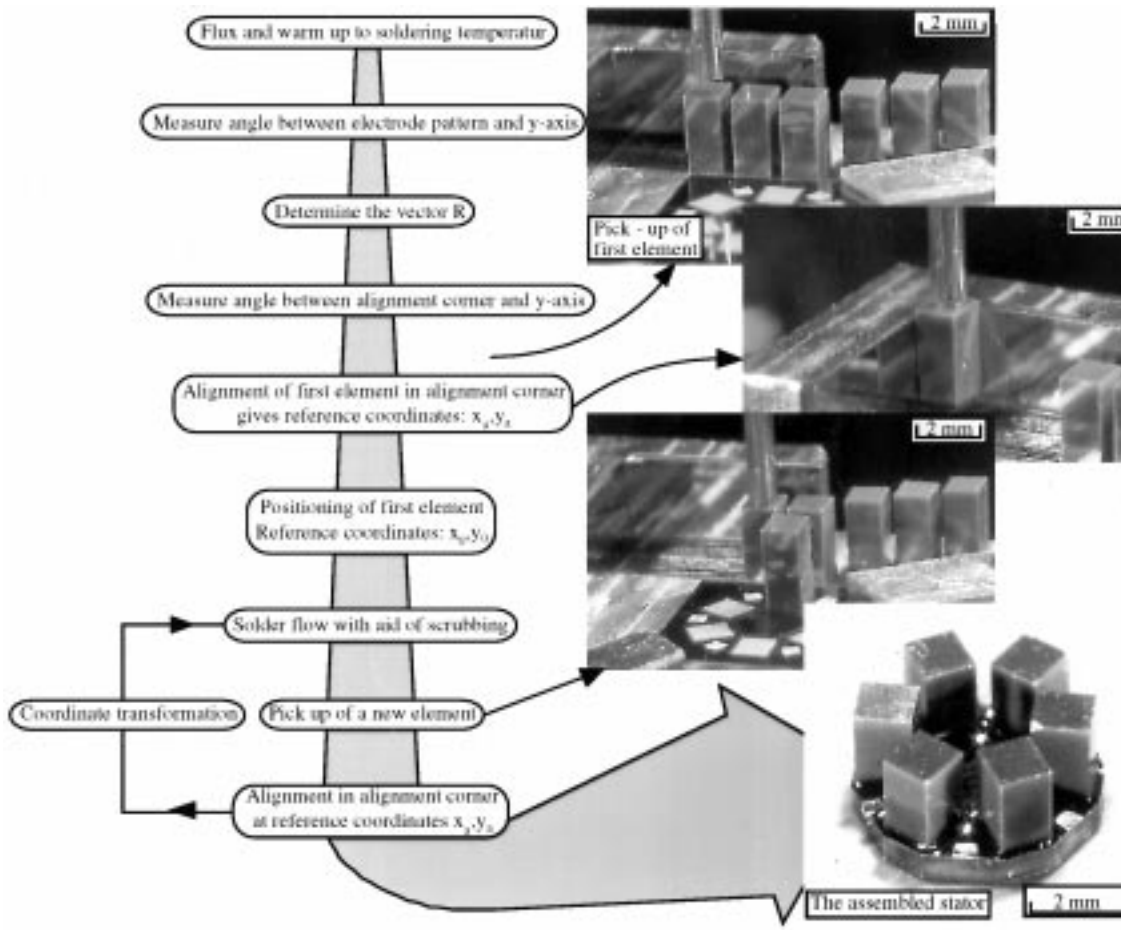


*Fig. 6.* Flow chart of the assembling sequence with illustrating photographs.

### *4.1. Coordinate Transformation*

The vacuum tool holding the piezoceramic elements is fixed at the same position during the whole assembling sequence. Hence the electrode pattern is moved to coincide with the electrodes in the piezoceramic elements. The coordinate transformations necessary for proper positioning of the electrode pattern is based on the symmetry of the electrode pattern. The electrode pattern has a six-fold symmetry, i.e., after a rotation of 60°, the pattern is identical. The hexagonal symmetry is clearly seen in e.g., Fig. 4(a). When the silicon substrate is clamped onto the heating table, the position for the electrode pattern is fixed in the *xy*-plane of the positioning stage. The rotational centre of the electrode pattern, E, in general does not coincide with the rotational axis, *S*, of the micropositioning stage. Figure 7 describes this case schematically where the hexagonal figure represents the electrode pattern. Since the two rotational centers are not aligned relative to each other, the center of the electrode pattern will follow a circular path around the rotational center for the positioning stage during rotation. The case for a 60° rotation is indicated in Fig. 8. The circle shows the trajectory for the centre of the electrode pattern. The full drawn hexagon shows the case before rotation and the hatched gray hexagon after rotation. The required translation to make these hexagons coincide is given by the vector $T$ in Fig. 8 which can be written as

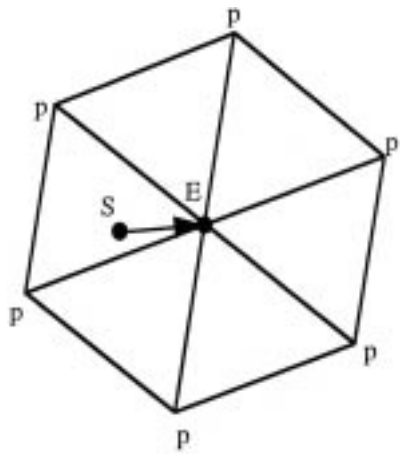


*Fig. 7.* Schematic drawing of the relation between position of the rotational centre for the micropositioning stage, S and the centre for the electrode pattern, E. The six points marked p are symmetry point in the electrode pattern.

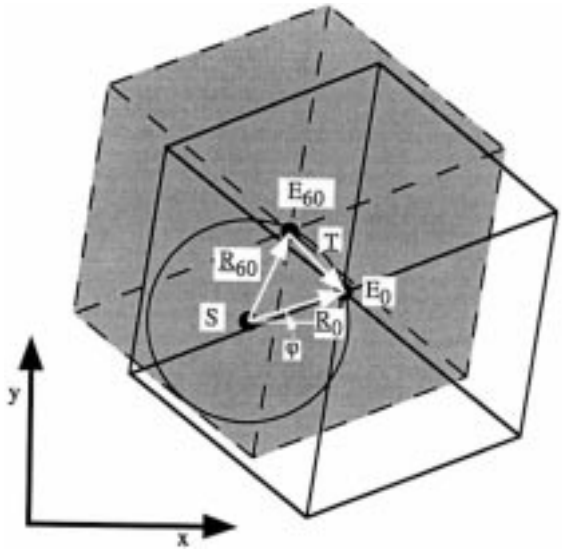


*Fig. 8.* The effect of a electrode pattern rotation when the centre of rotation does not coincide with the centre of the electrode pattern. Inserted are vectors of interest for the coordinate transformations.

$T = R_0 - R_{60}$ according to Fig. 8. If this is generalized and expressed in linear coordinates the required translation coordinates after rotation are given by

$$\begin{cases} x_\Theta = x_0 - |R_0|(\cos(\Theta + \varphi)) + |R_0|\cos(\varphi) \\ y_\Theta = y_0 - |R_0|(\sin(\Theta + \varphi)) + |R_0|\sin(\varphi) \end{cases} \tag{1}$$

where $\varphi$ is the angle between the $x$-axis and the vector $R_0$ (see Fig. 8), $x_0$ and $y_0$ are coordinates for an a convenient reference point. The angle $\Theta$ is chosen zero when the electrodes in one of the electrode areas are aligned with the $y$-axis since it is easier to create oscillations in a stage axis during solder wetting. Due to the six-fold symmetry of the electrode pattern, the angle of rotation, $\Theta$, will be an integer times 60° during assembly. $R_0$ and $\varphi$ are most easily determined by a rotation $\Theta$ of 180°.

### *4.2. Alignment of Piezoceramic Element in Alignment Corner and Subsequent Assembly*

In an automatic assembly sequence, it is a great advantage if the piezoceramic elements are held identically by the vacuum tool. This is accomplished here with an alignment corner on the heating plate. First, one side of the alignment corner is aligned with the $y$-axis according to Fig. 9. Then, a piezoceramic

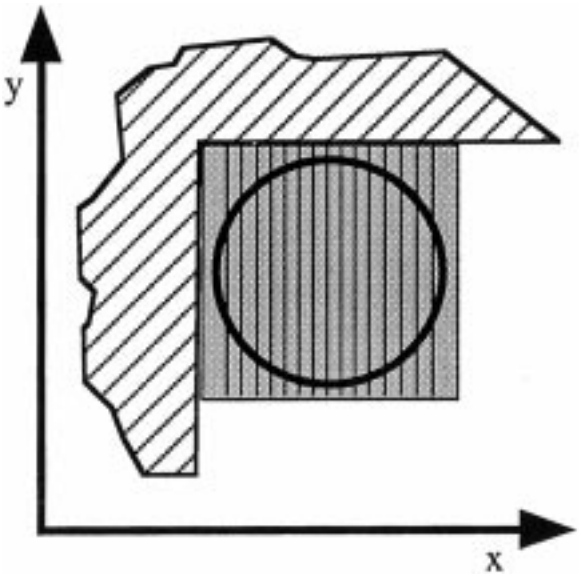


*Fig. 9.* Schematic drawing of the alignment procedure seen from above. The square represents the piezoceramic element and the circle the vacuum tool. One side in the alignment corner is aligned with the *y*-axis which makes the electrodes in the piezoceramic element aligned to the *y*-axis. The alignment corner is used to align the vacuum tool at the centre of the piezoceramic element.

element is picked up in such a way that after moving the corner towards the piezoceramic element diagonally, the vacuum tool will be centered at the top surface of the piezoceramic element. This procedure results in an identical orientation of the piezoceramic elements, both with respect to position and electrode alignment. The coordinates, $x_a$ and $y_a$, for the first piezoceramic element in the alignment corner are used as reference coordinates in the alignment of the remaining piezoceramic elements. Soldering of the first piezoceramic element is carried out according to the following sequence: Rotate the positioning table to align the electrodes in one of the electrode areas with the *y*-axis (defined as 0°). Position the piezoceramic element to make electrodes in piezoceramic element and electrode area coincide (by observation in the microscope). Coordinates $x_0$ and $y_0$ for this position is used as reference in further coordinate transformations. The spacing between the piezoceramic element and the silicon substrate is determined with the help of the force cell on the vacuum tool as will be discussed in section 5.3. While the piezoceramic element is held by the vacuum tool, the silicon substrate is oscillated in the *y*-direction to improve the flow of solder. Oscillations are made with a frequency of 1 Hz and an amplitude of $\pm$ 5 $\mu$m for 15–30 s.

### *4.3. Additional Fabrication Steps*

After assembling the stator, additional fabrication steps are needed in order to have a complete miniature motor. A two component epoxy underfill (EPO-TEK U300), cured at 120 °C for 15 min, is incorporated in the space between the piezoceramic element and the silicon substrate to improve the mechanical strength of the joint between the piezoceramic element and the silicon substrate. The resin is applied at one side of the piezoceramic element and, ideally, air should be pushed out in front of the resin minimizing the risk of air bubbles under the piezoceramic element. Sapphire plates are glued (with the same resin as above) onto the piezoceramic elements to serve as contact surfaces against the rotor and protect the piezoceramic elements from wear. The contact surfaces of the piezoceramic elements should ideally be in exactly the same plane. To minimize deviations from this ideal height, the stator was polished with the aid of a specimen disc grinder (Gatan model 623 disc grinder) and an extremely flat and hard polishing cloth. This resulted in a height error between piezoceramic elements of less then 200 nm. Electrical leads consisting of insulated copper wires were glued to the bonding pads (marked with X in Fig. 4(a)) with a silver adhesive. The stator is then bonded onto the baseplate with an adhesive. The ball bearing is pressed into the case. Thereafter the rotor is pressed into the ball bearing. Finally, the baseplate is screwed into the case in order to press the stator against the rotor.

## 5. Evaluation of Critical Assembly and Performance Parameters

### *5.1. Effect of Mechanical Scrubbing on Soldering*

The influence of mechanical scrubbing on soldering, i.e., an oscillating relative motion between the two surfaces to be soldered, was examined in-situ with the aid of an optical stereo microscope during soldering. Before scrubbing, the piezoceramic elements were placed at correct coordinates above the electrode areas and then pressed down to let the flux attack the oxide

and thereby induce solder flowing. At this stage it could be seen that on some electrodes solder already had started flowing. When the flowing had stopped, scrubbing was performed by oscillating the silicon substrate. Investigation of scrubbing were made with frequencies of 0.5, 1, 5 and 10 Hz, amplitudes of $\pm$ 1, $\pm$ 3 and $\pm$ 5 $\mu$m, and time of oscillation for 10, 30 and 60 s.

A typical example of how the solder has flowed along the Ag/Pd electrodes is given in Fig. 10. Solder is not seen on every Ag/Pd electrode surfaces in the figure which may be due to various reasons e.g., variations in flux effect on the sides of the piezoceramic element. During scrubbing it could be seen that flowing of the solder on the Ag/Pd electrodes increased. Generally it is believed that scrubbing assists with breaking oxides that obstruct soldering. An improved solder wetting on the Ag/Pd electrodes under the piezoceramic elements is therefore anticipated. It was observed that solder flow was more or less independent of amplitude and frequency of oscillation and after a time of approximately 15–30 s there was no further visible effect of scrubbing. The resulting frequency of 1 Hz and an amplitude of $\pm$ 5 $\mu$m for 15–30 s were used for scrubbing during assembly.

### *5.2. Angle Between Tip of Vacuum Tool and Electrode Pattern*

The soldering result is highly dependent on various alignment errors. In particular the influence of the angular error between the tip of the vacuum tool and the surface of the silicon substrate, Fig. 11, was investigated. This deviation error was measured for each assembling tests and in the three different series the angles were 2.5, 6 and 10 mrad. The plane parallelism of the piezoceramic elements is much less (about 0.1 mrad) and therefore does not influence the angular deviation. Soldering results were investigated by measuring the number of electrical failures of the 15 electrode connects between the piezoceramic elements and the electrode pattern.

It was found that the fraction of electrical failures depends on the deviation angle, see Table 1. Non soldered electrodes were typically outer electrodes in the piezoceramic element. The result can be explained by the relation between solder height and electrode pattern width. The height of the solder is about 5 $\mu$m and the distance between the outer electrodes in an piezoceramic element is 784 $\mu$m (a mean pitch of 56 $\mu$m). These figures give a maximum allowable deviation angle of about 6 mrad in order to have both outer electrodes in the piezoceramic element in contact with the solder. The measurements are in accordance with this. An angle of less then 6 mrad is needed to achieve good soldering, i.e., all electrodes in the piezoceramic element were soldered to the electrodes in the silicon substrate. It can be concluded that the angular error has to be less than a few mrad in order to achieve a sufficiently low failure probability.

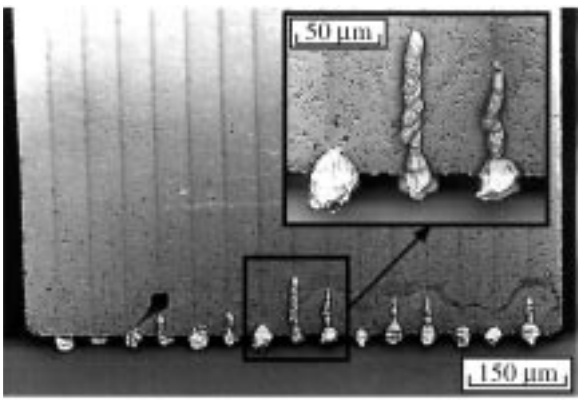


*Fig. 10.* An example of the good flowing characteristics for the Sn/Pb solder on the Ag/Pd electrodes. The close-up view of the solder alloy on the Ag/Pd surface shows how the solder typically has flown on the electrode surface.

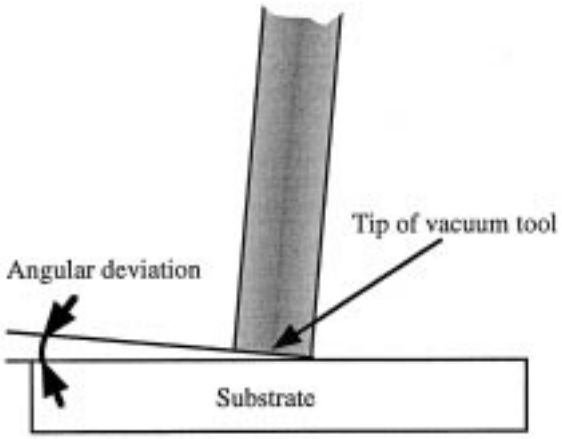


*Fig. 11.* Schematic drawing showing the most critical angular deviation between tip of vacuum tool and *xy*-plane of electrode pattern.

*Table 1*. Soldering results for different deviation errors between the tip of the vacuum tool and the silicon substrate surface. The failure probability is the fraction of electrical failures between the piezoceramic element and the electrode surface

| Deviation error (mrad) | Number of soldered actuator elements | Number of electrical connects | Number of electrical failures | Fraction electrical failures |
|---|---|---|---|---|
| $2.5 \pm 0.5$ | 4 | 60 | 0 | 0% |
| $6 \pm 0.5$ | 4 | 60 | 7 | 12% |
| $10 \pm 1$ | 2 | 30 | 10 | 33% |

*Table 2*. Results of soldering with different forces between piezoceramic element and silicon substrate

| Force (mN) | Number of soldered actuator elements | Number of electrical connects | Number of electrical failures | Fraction electrical failures |
|---|---|---|---|---|
| $6 \pm 2$ | 2 | 30 | 11 | 36% |
| $40 \pm 2$ | 4 | 60 | 0 | 0 |
| $60 \pm 2$ | 2 | 30 | 0 | 0 |
| $100 \pm 2$ | 2 | 30 | short circuit | short circuit |

### *5.3. Applied Force Between Piezoceramic Element and Silicon Substrate*

The demands on vertical positioning accuracy and sizes of the piezoceramic element could be reduced if the force between piezoceramic element and silicon substrate can be used as the feed-back parameter during assembly. Since the present polishing technique for the piezoceramic elements results in a size difference of the same order as the solder thickness, the possibility for feed-back from force measurements would be an important issue in an automatic process. The main object for the investigations was to determine if there is a relation between force and soldering results.

The number of electrical failures of the 15 electrode connects between the piezoceramic elements and the electrode pattern was measured for forces in the range 6–100 mN, Table 2. A direct correlation between force and fraction electrical failures can be seen. Soldering with too low a force gave electrode failures and with too high a force short circuits occurred. In the intermediate range, good soldering results were achieved. These results agree with what was expected, using too high a force, the solder expands laterally and eventually two adjacent electrodes get in contact and cause a short-circuit. Since the liquid solder can carry a certain load due to surface tension etc. there should be an intermediate range when the actuator electrodes have made contact with all solder lines before any short-circuit occurs. As a conclusion it appears to be possible to use force as a feed-back parameter in an automatic assembling sequence.

### *5.4. Examination of the Underfill*

To improve the mechanical strength of the piezoceramic elements, an underfill between piezoceramic element and the silicon substrate is used. The space is in the range of 3 to 10 $\mu$m and the fill properties of the underfill is therefore important. One commercially underfill (EPO-TEK U300) was examined with the aid of a wedge shaped spacing, consisting of two polished silicon plates separated 25 $\mu$m in one end and closed in the other. Silicon plates are used since they are extremely flat and easily available. A polished cross-section of the wedge was then examined in a scanning electron microscope (SEM). Also piezoceramic elements soldered to the silicon substrate were investigated with respect to fill properties and air bubble content in cross-section in the SEM. In all experiments cleaning was performed with acetone before gluing.

The investigation of the wedge shaped spacing showed that the resin filled a space that was narrower than 500 nm which is well below the spacing between piezoceramic element and silicon substrate. SEM investigation of the cross-section of the soldered piezoceramic element confirmed the expected behavior of the underfill. Very few air bubbles with the same size as the inter-electrode distance were present in an otherwise completely filled spacing.

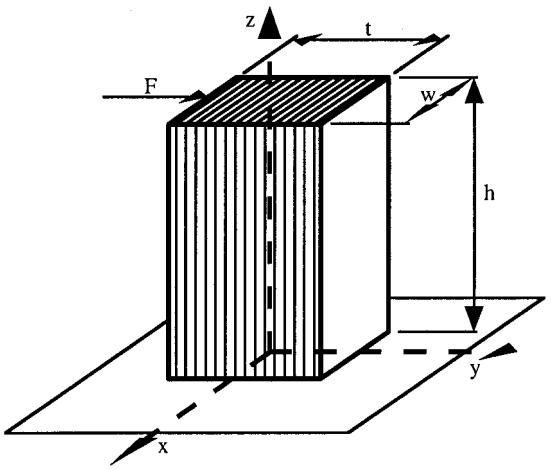


*Fig. 12.* Geometry of the measurement of joint strength between piezoceramic elements and silicon substrate.

### 5.5. *Joint Strength Measurement*

One of the factors that puts an upper limit on the motor torque is the joint strength between piezoceramic element and silicon substrate. The strength of the joints, with and without incorporation of an underfill, was measured by applying a horizontal force at the upper end of the piezoceramic element and registering the fracture limit. The micropositioning stage was used to position the piezoceramic elements and for applying the force. The sample was mounted in a special specimen holder with force cells for lateral measurements. The elements were tested against a fixed tool, shaped in order to get a well defined contact point. The maximum tensile stress is given by

$$\sigma_f = \frac{F_{\mathrm{f}} * h}{I_y/(t/2)} \tag{2}$$

where $F_f$ is the bending force at fracture, h is the height where the force is applied (1.4 mm in the experiments), $I_y$ is the moment of inertia of the cross-section perpendicular to the $z$-axis and t is the thickness of the element in the direction of the applied force ($y$-direction). The geometry for the fracture strength measurements is shown in Fig. 12. After fracture testing the fracture surfaces were examined in an SEM.

A typical fracture surface for a piezoceramic element without an underfill shows that the electrode film is separated from the silicon substrate. This indicates that adhesion between the electrode film and the silicon substrate is rather poor and partially explains the quite low fracture strength, of the order of 1 MPa. Using Eq. 2 it should be remembered that the electrode area is only a fraction of the total bottom area of the piezoceramic element. For this reason a resin is incorporated in the space between the piezoceramic element and the silicon substrate to improve the joint strength. A typical fracture surface for an underfill joint is exemplified with Fig. 13. Figure 13(a) shows the silicon substrate surface and

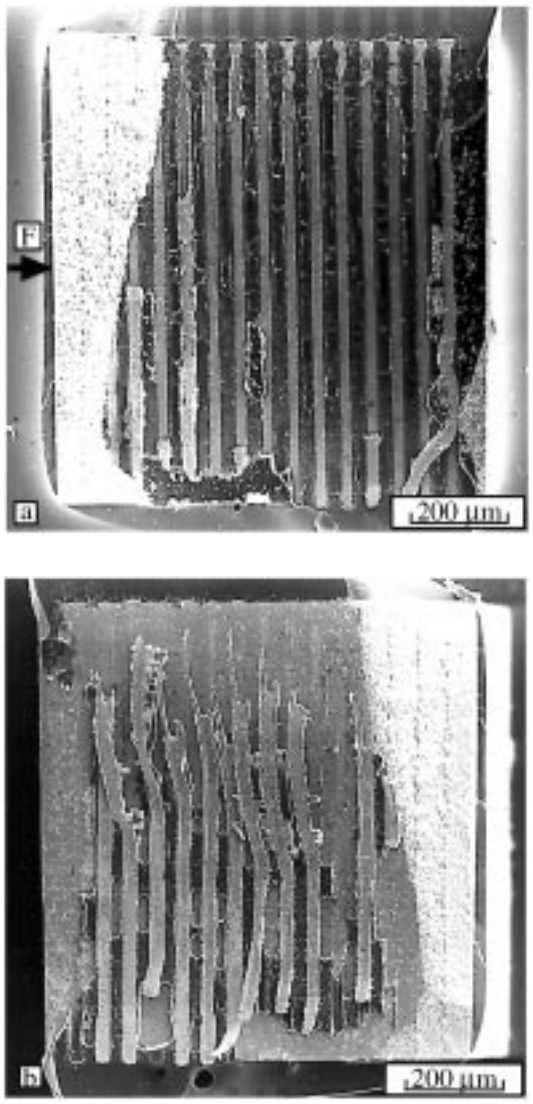


*Fig. 13.* SEM images of typical fracture surfaces for an underfilled piezoceramic element, showing (a) the remaining resin and ceramic residue on the silicon substrate and (b) corresponding surface of the piezoceramic element.

(b) the corresponding actuator surface. It can be seen that there is ceramic material from the piezoceramic element remaining on the silicon substrate surface. The force used to induce joint fracture has been applied from the left in Fig. 13(a), which is indicated with an arrow. It is also seen in Fig. 13(b) that the resin adheres very well to the ceramic since most of the underfill (darker areas at the ceramic surface) is left on the ceramic after fracture. Generally it is difficult to determine the cause of failure by studying a fracture surface. However, the ceramic residue at the silicon substrate shows that the fracture did not occur where the tensile stress is assumed to be highest (at the bottom near the silicon substrate), and that the ceramic fractured rather than the joint. Also, the ceramic residue was covered completely with resin (the underfill also covers the bottom part of the piezoceramic elements) while the remaining piezoceramic element was not. It appears reasonable to conclude that the resin has a strengthening effect on the ceramic material, which have been noticed before for brittle materials covered with a ductile film [9]. In the system piezoceramic element—resin—silicon substrate, the ceramic appears to be the weakest part. The measured joint strength for eight underfilled samples was $64 \pm 10$ MPa. It can be assumed that the maximum torque of the motor is limited by the mechanical weakest part which in this case seems to be the piezoceramic elements. With the design given in [8] the elements could support a torque level of 9 mNm. To investigate if the fracture strength could be increased further, some samples were completely covered with a cyano acrylate resin. The measured fracture strength was increased to about 100 MPa, which would allow for torque levels of up to 14 mNm. Fracture surfaces for these samples showed a similar appearance as the underfilled piezoceramic elements.

## Conclusions

An assembly method for the fabrication of a piezoelectric miniature motor has been presented. The fabrication was done by placement and soldering of piezoceramic elements onto a silicon substrate. The stator of the miniature motor was assembled with aid of a special micropositioning stage. A particular assembling sequence was used and critical process and performance parameters were evaluated. Mechanical scrubbing improved solder flow on the Ag/Pd electrodes. It was shown that an angle less than 6 mrad between the tip of the vacuum tool and the electrode pattern gave a soldering result with a sufficiently low failure probability. Possibilities for use of the applied force between the piezoceramic element and the silicon substrate as a feed-back parameter in an automatic assembling sequence was shown. One of the factors that puts an upper limit on the motor torque is the joint strength between piezoceramic element and silicon substrate. By using an underfill, a joint strength as high as 100 MPa has been measured. This would allow for torque values in the range of 14 mNm for a 4 mm diameter motor.

## Acknowledgments

Ulf Helin, Jonas Tirén, and Bengt Lindekvist, ABB HAFO have given us valuable help with the electroplating of the electrode pattern. The Industrial Microelectronics Center (IMC) have assisted with fabrication of the electrode pattern. The Swedish National Board for Industrial and Technical Development (NUTEK) and the Swedish Research Council for Engineering Science (TFR) supports the project financially.

## References

1. S. Johansson, Piezoelectric micromotor, Patent Appl. No. S 9300305-1 (1993).
2. M. Bexell, A.-L. Tiensuu, J.-Å. Schweitz, J. Söderkvist, and S. Johansson, *Sensors and Actuators*, **A43**, 322 (1994).
3. S. Uhea and Y. Tomikawa, *Ultrasonic motors—Theory and applications* (Clarendon Press, Oxford 1993), p. 1–4.
4. M. Bexell and S. Johansson, *in Proceedings Actuator 96*, edited by H. Borgmann (AXON Technologie Consult GmbH, Bremen, 1996), pp. 173–176.
5. S. Johansson, in *Materials Research Society Symposium Proceedings Volume 444: Materials for Mechanical and Optical Microsystems*, edited by M. L. Reed et al. (Materials Research Society, Pitsburgh, Pennsylvania, 1997), p. 3.
6. N. Koopman and S. Nangalia, in *Flip Chip Technologies* (Electronic Packaging and Interconnections Series), edited by J. H. Lau (McGraw-Hill, 1996), pp. 128–129, 132–134.
7. Epoxy Tecnology Inc., EPO-TEK 377, Specifications Rev. II.
8. M. Bexell and S. Johansson, to be published.
9. S. Johansson, F. Ericson, and J.-Å. Schweitz, *J. Appl. Phys.*, **65**(1), 122 (1989).